

Characterization of spun fibers with millimeter spin periods

Yong Wang and Chang-Qing Xu

Department of Engineering Physics, McMaster University, Hamilton, Ontario L8S 4L7, Canada
wangyong_w@yahoo.com yongw@mcmaster.ca

Viatcheslav Izraelian

IVG Fiber Ltd, 855 Alness Street, Toronto, Ontario, M3J 2X3, Canada

Abstract: Novel spun fibers with intrinsic asymmetric stress and millimeter spin periods are characterized both experimentally and theoretically. Based on the optical spectra of imprinted Bragg gratings, a new method is proposed to precisely measure their spin periods with a 0.1-mm spatial resolution. Properties of polarization-mode dispersion (PMD) and evolutions of polarization in these spun fibers are investigated. The intrinsic birefringence of spun fibers is then obtained with respect to the measured and simulated fiber PMD. Potential applications particularly in fiber sensing are discussed. It is shown that for these different applications, the requirements of fiber parameters are distinct.

©2005 Optical Society of America

OCIS codes: (060.2270) Fiber Characterization; (260.1440) Birefringence; (260.5430) Polarization

References

1. D. N. Payne, A. J. Barlow, and J. J. Ramskov-Hansen, "Development of low- and high- birefringence optical fibers," *IEEE J. Quantum Electron.* **18**, 477-486 (1982).
2. J. R. Qian, Q. Guo, and L. Li, "Spun linear birefringence fibres and their sensing mechanism in current sensors with temperature compensation," *IEE Proc-Optoelectron.* **141**, 373-380 (1994).
3. D. A. Nolan, X. Chen, and M. -J. Li, "Fibers with low polarization-mode dispersion," *J. Lightwave Technol.* **22**, 1066-1077 (2004).
4. A. Pizzinat, L. Palmieri, B. S. Marks, *et al.*, "Analytical treatment of randomly birefringent periodically spun fibers," *J. Lightwave Technol.* **21**, 3355-3363 (2003).
5. S. M. Pietralunga, M. Ferrario, P. Martelli, *et al.*, "Direct observation of local birefringence and axis rotation in spun fiber with centimetric resolution," *IEEE Photon. Technol. Lett.* **16**, 212-214 (2004).
6. A. Galtarossa, L. Palmieri, and D. Sarchi, "Measure of spin period in randomly birefringent low-PMD fibers," *IEEE Photon. Technol. Lett.* **16**, 1131-1133 (2004).
7. Y. Wang, C. -Q. Xu, and V. Izraelian, "Characteristics of fiber Bragg gratings in spun fibers," *Proc. SPIE* **5577**, 262-272 (2004).
8. J. Sakai and T. Kimura, "Birefringence and polarization characteristics of single-mode optical fibers under elastic deformations," *IEEE J. of Quantum Electron.* **17**, 1041-1051 (1981).
9. B. L. Heffner, "Automated measurement of polarization mode dispersion using Jones matrix eigenanalysis," *IEEE Photon. Technol. Lett.* **4**, 1066-1069 (1992).
10. R. C. Jones, "A new calculus for the treatment of optical systems. IV. Experimental determination of the matrix," *J. Opt. Soc. Am.* **37**, 110-112 (1947).
11. Y. Wang, C. -Q. Xu, and V. Izraelian, "Bragg gratings in spun fibers," *IEEE Photon. Technol. Lett.* (to be published).
12. A. Othonos, K. Halli, *Fiber Bragg Gratings: Fundamentals and Applications in Telecommunications and Sensing* (Artech House, Boston, 1999).

1. Introduction

Low-birefringence fibers are in high demand in the current high-speed optical transmission systems [1], and polarization-independent components are also required in many high-accuracy fiber-optic sensing networks [2]. As a result, polarization-insensitive transmission fibers and components have been pursued recently. To investigate the detrimental effect of fiber birefringence, the polarization-mode dispersion (PMD) is usually taken as a measure of the difference in propagation time of two orthogonal states of polarization (SOP) in fibers. There are usually two methods to reduce fiber PMD and birefringence. One is to eliminate asymmetries in the fiber index and stress profiles; the other is to rotate fibers in the manufacturing process, known as spun fibers, which has been proven to be very effective to reduce the PMD [3]. Several analytic models have been deduced to study mode propagation and PMD in spun fibers with different fiber birefringence [3,4]. In experiments, Pietralunga, *et al.* recently traced the SOP along a spun fiber with a spin period of 46 cm using the cut-back method [5]. Lately, Galtarossa, *et al.*, adopted a polarization-sensitive optical time-domain reflectometer (POTDR) based technique to measure spin periods of some spun fibers with a relatively low spatial resolution (0.5 m) [6]. At present, the spin periods of spun fibers have been successfully reduced to a scale of a few millimeters [7]. However, neither method above can be used to measure these millimeter spin-period spun fibers. In this paper, a new method is proposed to precisely measure short spin periods with a spatial resolution of 0.1 mm. More importantly, the spun fibers with such millimeter spin periods and intrinsic birefringence are found to have many novel characteristics compared to the conventional single-mode fibers, and some potential applications are discussed.

2. Experimental results

The spun and unspun fibers investigated in this work were drawn from an asymmetric preform that has a D-shaped cladding and a round core in the center. For the unspun fiber, it has a symmetric structure – a round cladding and a round core at the center – due to surface tension in the manufacturing process at a high temperature of above 1000 °C. However, nonuniform stress in the fiber cross section as depicted in Fig. 1(a) introduces some birefringence into the fiber. The spun fibers subsequently drawn from the same preform may still have some intrinsic stress inside the fibers, but at reduced amplitudes, which is discussed quantitatively in the next section. From a classic analysis of spun fibers [8], the intrinsic stress in these spun fibers may have approximately a spiral structure with a spin rate of α (turns/m) in the longitudinal direction as schematically shown in Fig. 1(b). Therefore, we can change the amplitude of intrinsic birefringence (Δn_L) and spin rate (α) in a spun fiber by controlling the polishing depth of preform and the drawing speed of fiber, respectively. Here, (x, y, z) denotes a fixed coordinate system, while ξ and ζ represent the local rotation coordinates with respect to the slow and fast axes of fiber. As a signature, the introduced stress may offer some novel properties of polarization, and help us to investigate the spinning characteristics of fiber. These are detailed later in this paper.

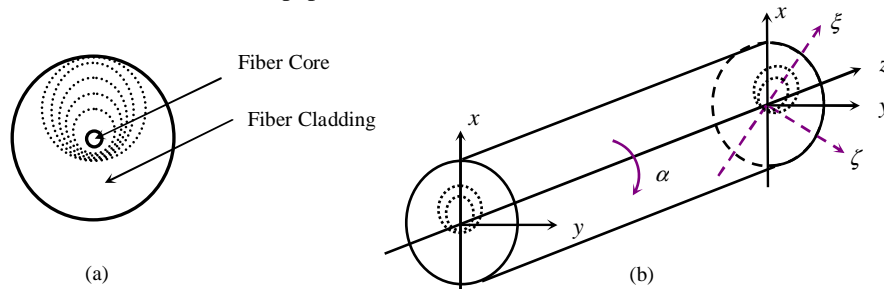


Fig. 1. (a) Schematic stress distribution in cross section of unspun fiber. (b) Evolution of intrinsic stress in a spun fiber.

One unspun fiber (namely, #1) and four spun fibers (namely, #2-5) with spin periods of 1.7 ~ 3.2 mm and lengths of tens of meters were studied. The spin periods of these fibers are precisely given in Table 1, whose determination is based on a grating-assisted spectral method and discussed later. For each spun fiber examined in this work, the spin rate is constant in the drawing process, and the fiber core and cladding diameters are ~8.0 and ~125 μm , respectively.

Table 1. Spin periods and unit-length fiber PMD.

Fibers	# 1	# 2	# 3	# 4	# 5
P_s (mm)	∞	1.78	2.25	2.94	3.16
PMD (ps/m)	0.363	0.0189	0.0218	0.0272	0.0290

The spiral stress structures in the four spun fibers have been observed through optical microscopical images, as exemplified in Fig. 2 for spun fiber # 3 with fiber coating stripped off. When the objective lens is focused onto the top surface of cladding and into the fiber core, as shown in Fig. 2(a)-(b), respectively, we can see similar shapes of core and cladding to those of a traditional single-mode fiber. However, with the microscope focused onto a layer below the core, an apparent periodical pattern of refraction alternatively in orange and blue along the spun fiber can be seen with illumination of a white light. In particular, a segment of fiber corresponding to such a half period is depicted in Fig. 2(c), where the distance between two spot centers (A_1 and A_2) is measured to be ~1.1 mm. The magnified fiber images around spots A_1 and A_2 are shown in Fig. 2(d)-(e), exhibiting two opposite mappings of color. From physical optics, distinct colors of refraction correspond to different profiles of refractive index, which implies concave- or convex-like index distributions surrounding the fiber axis in the spun fiber. Furthermore, when slightly rotating the fiber along its longitudinal axis, the opposite refraction patterns synchronously move along the fiber. These phenomena confirm a spiral structure of intrinsic stress surrounding the fiber core, as previously analyzed and plotted in Fig. 1(b). In addition, it is worth noting that the spin periods read out under the microscope are not accurate enough, due to a strong dependence of human judgment on spot centers.

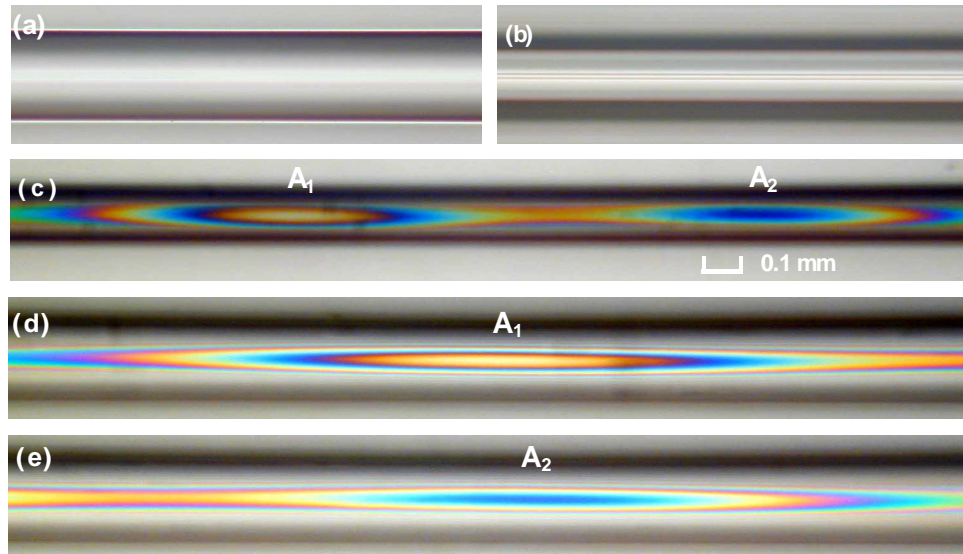


Fig. 2. Microscopical images of spun fiber # 3 focused on (a) top surface of cladding, (b) fiber core, (c) bottom. (d)-(e) Magnified images around points A_1 and A_2 in (c).

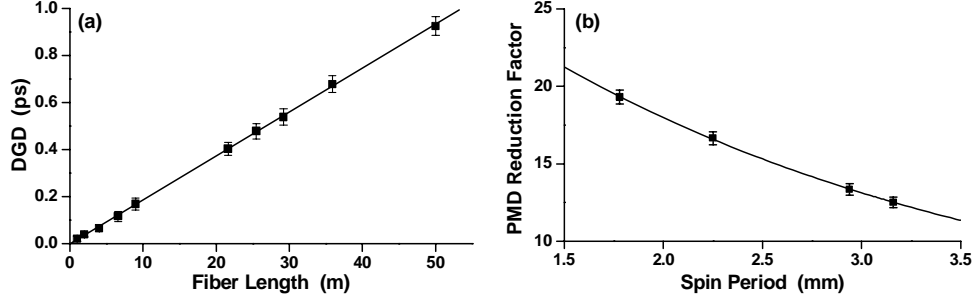


Fig. 3. (a) DGD versus fiber length for spun fiber #2. (b) PMD reduction factor versus spin period.

The fiber PMD values in a unitary length are also shown in Table 1. For these fibers, the feasibility of calculating the unit-length differential group delay (DGD) from a total DGD obtained with Agilent 8509C is guaranteed due to such a fact that for each fiber, the fiber DGD grows almost linearly with fiber length in a range of up to 50 m as observed in the experiment using the cut-back method and typically shown in Fig. 3(a) for fiber #2. We can see in Table 1 that compared with the unspun fiber, the fiber spinning can effectively eliminate fiber PMD, and the spun fiber PMD can be further reduced with a decrease of spin period. The reduction of PMD can hence be quantified by adopting PMD reduction factor denoted as a ratio of unit-length DGD of a spun fiber to that of the unspun fiber drawn from the same preform, and depicted in Fig. 3(b) for spun fibers #2-5 with an exponential fitting. For each of the spun fibers, the PMD reduction factor exceeds 10; and the shorter the period, the higher the factor.

3. Theory and simulation

The polarization characteristics and SOP evolutions in spun fibers can be further investigated in terms of theory and simulation. The x - and y -polarized modes (HE_{11}^o and HE_{11}^e) that are mutually normal modes in an unspun fiber can be coupled to each other in a spun fiber. Regardless of the transmission loss, the behavior of mode coupling is governed by the following coupled-mode equation (CME) [2,8]

$$\frac{d}{dz} \begin{bmatrix} E_x \\ E_y \end{bmatrix} = -j \begin{bmatrix} \beta_0 + 0.5\Delta\beta_L \cos(2\alpha z) & 0.5\Delta\beta_L \sin(2\alpha z) \\ 0.5\Delta\beta_L \sin(2\alpha z) & \beta_0 - 0.5\Delta\beta_L \cos(2\alpha z) \end{bmatrix} \begin{bmatrix} E_x \\ E_y \end{bmatrix} \quad (1)$$

where E_x and E_y are the amplitudes of two coupled modes polarized in the x and y directions, respectively. β_0 is the average propagation constant of the two normal modes, and $\Delta\beta_L$ corresponds to the intrinsic linear birefringence (Δn_L). The spin rate α is equal to $1/P_s$ (P_s is the spin period). By taking the matrix transformation,

$$\begin{bmatrix} E_x \\ E_y \end{bmatrix} = \begin{bmatrix} \cos(\alpha z) & -\sin(\alpha z) \\ \sin(\alpha z) & \cos(\alpha z) \end{bmatrix} \begin{bmatrix} E_\zeta \\ E_\xi \end{bmatrix} \quad (2)$$

we obtain the CME in a rotation coordinate system (ζ, ξ),

$$\frac{d}{dz} \begin{bmatrix} E_\zeta \\ E_\xi \end{bmatrix} = -j \begin{bmatrix} \beta_0 + 0.5\Delta\beta_L & \alpha \\ -\alpha & \beta_0 - 0.5\Delta\beta_L \end{bmatrix} \begin{bmatrix} E_\zeta \\ E_\xi \end{bmatrix}. \quad (3)$$

With three constants β_0 , $\Delta\beta_L$ and α , the two eigenvalues of Eq. (3), i.e., $\beta_0 \pm [\Delta\beta_L^2/4 + \alpha^2]^{1/2}$, correspond to the propagation constants of two eigenmodes in the rotation coordinate system, and are independent of propagation distance z . Therefore, the electric fields in the fixed coordinate system become

$$\begin{bmatrix} E_x(z) \\ E_y(z) \end{bmatrix} = \begin{bmatrix} \cos(\alpha z) & -\sin(\alpha z) \\ \sin(\alpha z) & \cos(\alpha z) \end{bmatrix} \begin{bmatrix} \cos(\rho z) - j \frac{\Delta\beta_L}{2\rho} \sin(\rho z) & \frac{\alpha}{\rho} \sin(\rho z) \\ -\frac{\alpha}{\rho} \sin(\rho z) & \cos(\rho z) + j \frac{\Delta\beta_L}{2\rho} \sin(\rho z) \end{bmatrix} \times \begin{bmatrix} E_x(0) \\ E_y(0) \end{bmatrix} \exp(-j\beta_0 z) \quad (4)$$

with $\rho = [\Delta\beta_L^2/4 + \alpha^2]^{1/2}$. Using Eq. (4), we can investigate the evolutions of SOP in these spun fibers. With $|E_x(z)|^2 + |E_y(z)|^2 = 1$, the total power in spun fibers is conservative despite the mode coupling.

Furthermore, the fiber PMD is measured and calculated with the Jones matrix eigenanalysis method [9]. The transmission Jones matrix of an unknown device can be obtained usually by measuring three output Jones vectors in response to three known stimulus polarizations [10]. Here, for a fiber with a length of L , the measurement is the simplest when three linearly polarized Jones vectors oriented at 0° , 90° and 45° , i.e. $[1, 0]^T$, $[0, 1]^T$ and $[1, 1]^T/\sqrt{2}$ are adopted, and the three corresponding output Jones vectors are denoted by $[E_{x1}(L), E_{y1}(L)]^T$, $[E_{x2}(L), E_{y2}(L)]^T$ and $[E_{x3}(L), E_{y3}(L)]^T$, respectively. The normalized Jones matrix \mathbf{T} is then given by [10]

$$\mathbf{T} = \begin{bmatrix} k_1 k_4 & k_2 \\ k_4 & 1 \end{bmatrix} \quad (5)$$

$$k_1 = \frac{E_{x1}(L)}{E_{y1}(L)}, \quad k_2 = \frac{E_{x2}(L)}{E_{y2}(L)}, \quad k_3 = \frac{E_{x3}(L)}{E_{y3}(L)}, \quad k_4 = \frac{k_3 - k_2}{k_1 - k_3}. \quad (6)$$

The DGD $\Delta\tau$ can hence be expressed as

$$\Delta\tau = \left| \frac{\text{Arg}(\rho_1 / \rho_2)}{\Delta\omega} \right| \quad (7)$$

where Arg denotes the argument function, $\Delta\omega$ is the step size in terms of angular frequency ω , and ρ_1 and ρ_2 are the eigenvalues of the matrix product $\mathbf{T}(\omega + \Delta\omega)\mathbf{T}^{-1}(\omega)$. The eigenvectors of this product correspond to the principal states of polarization (PSPs) of a fiber, and the PMD is determined by the dispersion vector with an amplitude of $\Delta\tau$ and a direction of a PSP.

By using Eq. (7), the spun fiber DGD versus fiber length is firstly calculated for different intrinsic linear birefringence of 0.5×10^{-4} and 1.0×10^{-4} , and spin periods of 2.0 and 4.0 mm, and shown in Fig. 4(a). The wavelength is 1550 nm, and the step size is 10 pm. We can see that the fiber DGD varies linearly with fiber length in a range of up to 50 m, which is in good agreement with the measured results shown in Fig. 3(a). Each curve has a different slope corresponding to the so-called unit-length DGD. Of course, a lower intrinsic birefringence or a shorter spin period leads to a lower DGD. With such a linear dependence of PMD on fiber length, only the PMD in a unitary length is discussed next. For these four cases I-IV, the unit-length DGD versus wavelength is then plotted in Fig. 4(b). One can see that the fiber DGD is nearly independent of wavelength in the range of 1530-1570 nm, which allows us to consider a small wavelength range, for example, near 1550 nm, in the following simulation.

The dependence of unit-length fiber DGD on intrinsic birefringence and spin period near 1550 nm is shown in Fig. 5 on both linear and logarithmic scales. It is seen that with a decrease of spin period or intrinsic birefringence, the fiber DGD drops. In particular, the DGD exhibits a nearly linear relation with spin period for $\Delta n_L > 0.5 \times 10^{-4}$, and an approximately exponential relation for $\Delta n_L < 0.5 \times 10^{-4}$. For telecommunication applications, low fiber PMD is always pursued, which requires the adoption of relatively low intrinsic birefringence and short spin period. In particular, when the fiber birefringence drops to a level of 10^{-6} (a beat length of ~ 1.5 m at 1550 nm), the fiber PMD can be reduced to a level of 0.1 ps/km even with

a rather long spin period of > 1 m. Moreover, it was found that in contrast with a constant spin rate, a periodically modulated spin rate particularly in a sinusoidal manner may further suppress fiber PMD [3]. These properties render the spun fibers more suitable for long-haul and high-speed transmission than those unspun fibers. For fiber sensing applications, the requirement for low PMD can be greatly relaxed since the lead fibers of sensors are usually not very long, and the fiber PMD is somehow not critical to affect sensor performance.

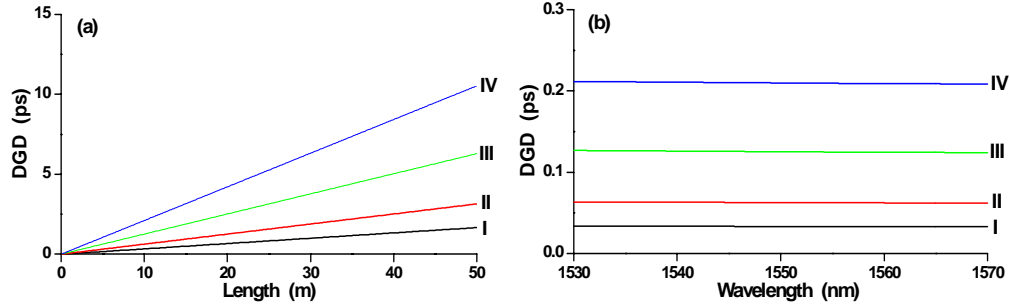


Fig. 4. (a) Fiber PMD versus fiber length and (b) unit-length fiber PMD versus wavelength for different birefringence and spin periods. (I) $\Delta n_L = 0.5 \times 10^{-4}$, $P_s = 2.0$ mm, (II) $\Delta n_L = 0.5 \times 10^{-4}$, $P_s = 4.0$ mm, (III) $\Delta n_L = 1.0 \times 10^{-4}$, $P_s = 2.0$ mm, (IV) $\Delta n_L = 1.0 \times 10^{-4}$, $P_s = 4.0$ mm.

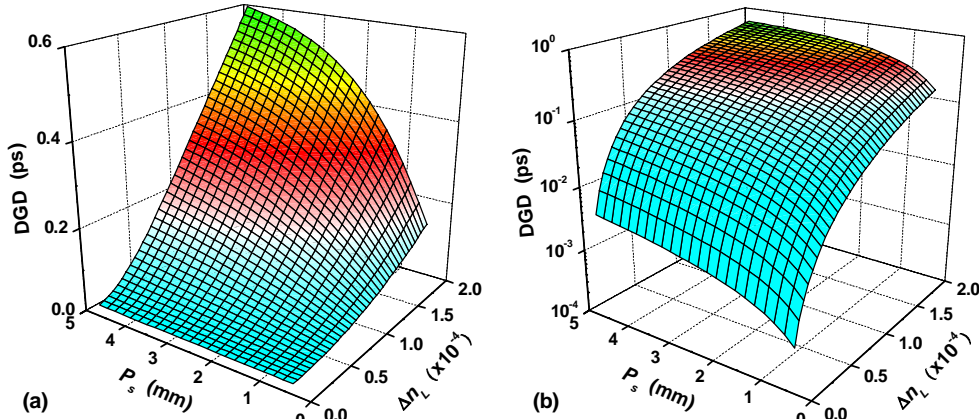


Fig. 5. Unit-length fiber PMD versus birefringence and spin period on (a) linear and (b) logarithmic scales.

Based on the calculated results of fiber PMD shown in Fig. 5 and the measured data given in Table 1, the practical intrinsic fiber birefringence (Δn_L) can be determined using the least squares method. Here, we define an estimation function as

$$F(\Delta n_L) = \sum_{i=1}^4 [\Delta \tau(\Delta n_L, P_{s,i}) - \Delta \tilde{\tau}(P_{s,i})]^2 \quad (8)$$

where $i = 1, \dots, 4$, refer to spun fibers #1-4 with spin periods of $P_{s,i}$. $\Delta \tau$ is calculated from Eq. (7), and the measured value $\Delta \tilde{\tau}$ is from Table 1. F is then drawn in Fig. 6(a) on a logarithmic scale as a function of linear birefringence Δn_L in the range from 2.0×10^{-4} to 6.0×10^{-4} . A sharp notch occurs on F at $\Delta n_L = 0.378 \times 10^{-4}$, implying a fairly accurate estimation of intrinsic birefringence for these spun fibers. It is further found that the estimation uncertainty of Δn_L is $< 10^{-7}$. Substituting $\Delta n_L = 0.378 \times 10^{-4}$ in Eq. (7), we obtain the relation between fiber DGD and spin period for the practical spun fibers, which is shown in Fig. 6(b) together with the measured results. Good agreement between the simulated and measured results further validates the adopted model for these spun fibers.

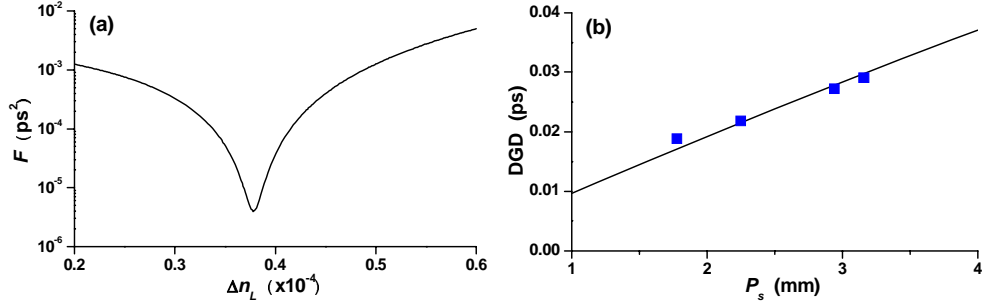


Fig. 6. (a) F as a function of linear birefringence. (b) Comparison between simulated (solid line) and measured (squares) results.

Meanwhile, the linear birefringence of the unspun fiber (fiber #1) was measured to be 1.0×10^{-4} by examining its beat length through a Sagnac interferometric method [7]. One can see that the intrinsic linear birefringence of the spun fibers is smaller than that of the unspun fiber approximately by a factor of 3. This is different to a common assumption – the birefringence of a spun fiber is the same as that of an initial unspun fiber – extensively adopted in the previous models and analyses [2,3,8]. This difference could be understood by considering the internal tension in the fiber drawing process at a temperature in excess of 1000° . During a very fast spinning, the strong twisting tension in the fused silica tends to mitigate the initial stress or birefringence; whereas in a slow spinning, the mitigating effect caused by the twisting tension is weakened. The intrinsic birefringence hence may not decrease significantly in those spun fibers with long spin periods. Furthermore, using the Sagnac interferometric method [7], the beat length was measured to be 28, 23, 18 and 17 cm for spun fibers #2-5, corresponding to the effective birefringence of $5.6, 6.8, 8.7$ and 9.0×10^{-6} , respectively. Since the intrinsic birefringence in these spun fibers is higher than the effective birefringence by at least one order of magnitude, the averaging effect of spinning is prominent in these spun fibers.

4. Applications and discussion

We have investigated the PMD properties of the spun fibers with millimeter spin periods, and found that the fiber PMD depends on both the intrinsic birefringence and spin period. By comparing the measured and simulated results, we have precisely characterized the intrinsic birefringence of the spun fibers. In this section, we discuss the novel properties of spun fibers and their potential applications especially in fiber sensing.

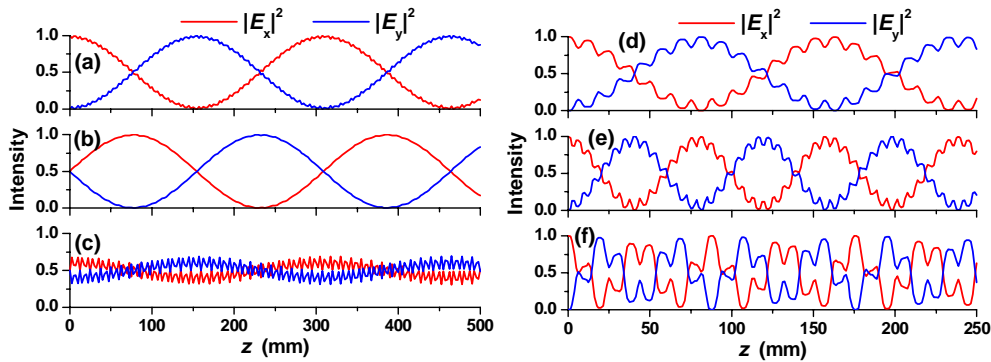


Fig. 7. Evolutions of SOP in spun fibers with different birefringence, spin periods and input SOP. (a) $\Delta n_L = 0.5 \times 10^{-4}$, $P_s = 2.0$ mm, 0° linearly polarized input; (b) $\Delta n_L = 0.5 \times 10^{-4}$, $P_s = 2.0$ mm, 45° linearly polarized input; (c) $\Delta n_L = 0.5 \times 10^{-4}$, $P_s = 2.0$ mm, right-circularly polarized input; (d) $\Delta n_L = 0.5 \times 10^{-4}$, $P_s = 4.0$ mm, 0° linearly polarized input; (e) $\Delta n_L = 1.0 \times 10^{-4}$, $P_s = 2.0$ mm, 0° linearly polarized input; (f) $\Delta n_L = 1.0 \times 10^{-4}$, $P_s = 4.0$ mm, 0° linearly polarized input.

From Eq. (4) the evolutions of polarization in spun fibers can be obtained, and are plotted in Fig. 7 for typical fiber birefringence and spin periods. With $\Delta n_L = 0.5 \times 10^{-4}$, $P_s = 2.0$ mm, the normalized field amplitudes as functions of propagation distance are depicted in Fig. 7(a)-(c) for three different SOP, i.e., 0° and 45° linear polarizations and a right-circular polarization, respectively. Despite different features in the three cases, the polarization evolutions exhibit the same major spatial period and some higher-frequency components. This major spatial period is 30.9 cm, and denoted by the conversion length L_{conv} , at which the optical power converts alternatively between two orthogonal directions (x and y). The magnitudes of power oscillation or conversion are different for the linear and circular polarizations. For the former, a 100% conversion can be realized in lieu of a 30% conversion for the latter. With an increase of Δn_L or P_s as shown in Fig. 7(d)-(f), this major spatial period decreases accompanied by more prominent higher-frequency components. Correspondingly, L_{conv} is 15.9, 8.0 and 4.4 cm in Fig. 7(d)-(f), respectively. Besides the major spatial periods, the second-order spatial periods can also be read out, which are 12.6, 6.3 and 12.6 mm in Fig. 7(d)-(f), respectively. Using the Fourier transform with respect to fiber distance, we can obtain the spectrum of spatial period. From a spectrum analysis on Eq. (4), we find that the frequency components are mainly composed of $(\rho-\alpha)/\pi$, α/π and $(\rho+\alpha)/\pi$, and the corresponding spatial periods are $\pi/(\rho-\alpha)$, π/α and $\pi/(\rho+\alpha)$. Compared with the former two, the amplitude of the third frequency component $(\rho+\alpha)/\pi$ is very small, and hence negligible. It is further found that $\pi/(\rho-\alpha) > \pi/\alpha$ holds for all cases in Fig. 7, consequently $\pi/(\rho-\alpha)$ corresponds to the major spatial period (L_{conv}), and π/α determines the second-order harmonic. When $\Delta n_L \cdot P_s > \sqrt{3}\lambda/\pi$ is satisfied, we have $\pi/(\rho-\alpha) < \pi/\alpha$. In this case, the competition between two spatial periods may occur.

Based on the Fourier transform, the conversion length L_{conv} is then calculated as a function of spin period and fiber birefringence, and plotted in Fig. 8. We can see that in the given parameter ranges, L_{conv} rapidly drops from hundreds to tens of millimeters with an increase of P_s or Δn_L . In particular, L_{conv} is less than 50 mm for either $\Delta n_L \geq 1.0 \times 10^{-4}$ or $P_s \geq 3.0$ mm. In the ranges of $1.6 \times 10^{-4} < \Delta n_L \leq 2.0 \times 10^{-4}$ and $4.2 < P_s \leq 5.0$ mm, L_{conv} reaches a minimum value of ~ 13.5 mm along the curve $\Delta n_L \cdot P_s = \sqrt{3}\lambda/\pi$. With $\Delta n_L \cdot P_s > \sqrt{3}\lambda/\pi$, the conversion length is mainly determined by the spin rate rather than birefringence. It can be easily understood that in this case with certain birefringence and enough long spin period, the performance of these spun fibers look more like traditional Hi-Bi fibers under a twist. In fact, the two orthogonal polarization modes can be maintained in the rotation coordinate system (ξ and ζ) with a twist rate of α .

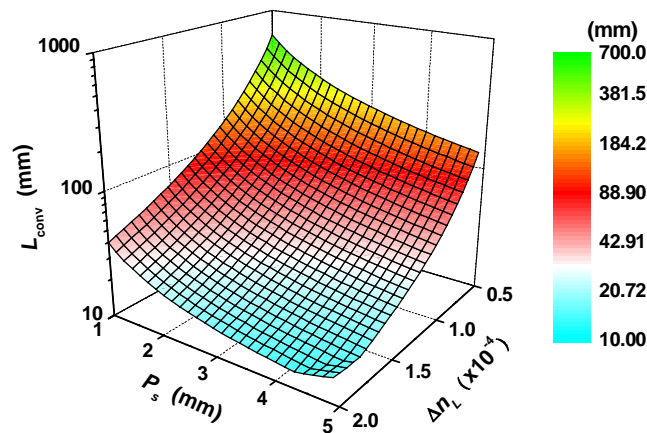


Fig. 8. Polarization conversion length versus linear birefringence and spin period.

We have exemplified that the two orthogonal modes in a spun fiber exchange their powers within a conversion length. This property can enable a spun fiber to have a certain resistance to external perturbations, such as nonuniform lateral stress caused by side pressure or bending, nonuniform refractive index change caused by side UV exposure, etc., and to maintain the original polarization characteristics. It is well known that in a traditional fiber, an external perturbation usually impacts more on one mode or polarization than the other; as a result, a fiber always exhibits a certain polarization dependence on external effects. For a spun fiber device used in a transmission manner, if a fiber section suffering from a lateral perturbation is longer than the conversion length, the two orthogonal modes may experience the same perturbation, and consequently weaken the influence of perturbation. Of course, the external perturbation should not be too strong to apparently change the fiber modes. In particular, the fiber geometric structure should still be kept approximately symmetric, and the perturbation-induced birefringence should be much less than the original linear birefringence (Δn_L). For many fiber devices particularly in fiber sensing, such as fiber Bragg grating (FBG) sensors, both FBGs and their lead fibers may be subject to a variety of external perturbations in practical applications. Meanwhile, a traditional FBG itself also suffers from an uneven index change in its cross section due to side UV exposure in the FBG fabrication. Therefore, to effectively compensate the UV-induced birefringence in a spun fiber, its conversion length should be shorter than the FBG length. Since the lengths of most FBGs are in the range from several millimeters to tens of millimeters, to reduce L_{conv} to this level, one needs to adopt a relatively long P_s (~ 4 mm) and relatively high Δn_L ($\sim 10^{-4}$). The polarization-insensitive fiber gratings need a further study, and more results will be presented elsewhere. Moreover, these results are also consistent with the previous analysis that a spun fiber with a high spin rate and low birefringence is sensitive to fiber bending and applied stress [1,2].

It is worth noting that the requirement for a high fiber resistance to external perturbations is different to that for low fiber PMD. The former requires high Δn_L and a long P_s , while the latter does the contrary. Therefore, the selection of the spun fiber parameters is dependent on a practical application. In the following discussion, we will illustrate some novel characteristics of FBGs imprinted in spun fibers #2-5 as well as their potential applications. Since some experimental and simulation results of spun FBGs have been presented in [11], here we focus on the fiber properties and basic requirements for these applications.

To fabricate FBGs, these spun fibers with a similar germanium concentration to a conventional single-mode fiber were side-exposed to uniform UV light at 248 nm through a holographic phase mask with a pitch of 1064.82 nm after 3-week hydrogen loading at a 1500-psi pressure. Typical optical spectra of transmission and reflection are shown in Fig. 9(a) for a 15-mm long FBG in spun fiber #2. In this test, a broadband light source and an optical spectrum analyzer (Ando AQ6317) were used. The transmission spectrum is similar to a uniform FBG in a traditional single-mode fiber. However, in the reflection spectrum, multiple peaks appear near the Bragg wavelength (λ_B), and their wavelength intervals are 0.46 nm. From the Bragg peak (P_B), these side peaks are denoted in turn by $P_{\pm 1}$, $P_{\pm 2}$, etc. One can see that side peaks $P_{\pm 1}$ and $P_{\pm 2}$ are dominant, and the others are much weaker. Furthermore, we find that the multiplex phenomena apply to all these spun fibers, but with different wavelength intervals of 0.46, 0.37, 0.28 and 0.26 nm for spun fibers #2-5, respectively. When a narrow-linewidth and polarized tunable laser (HP 81642A) and an optical power meter were used to measure the reflection spectra of spun FBGs, it was found that the reflection peaks had different polarization dependences on input SOP. In particular, the polarization dependence is about 0.1-0.2 dB for P_B , 1.0-2.0 dB for $P_{\pm 1}$, and 4.0-6.0 dB for $P_{\pm 2}$.

The generation of the multiple peaks in spun FBG reflection spectra is attributed to longitudinal modulations of index change. When the UV light is side-exposed onto a spun fiber, the interaction with the aforementioned spiral stress shown in Fig. 2(c) can lead to a longitudinal modulation of refractive index change with two sets of periodical structures, characterized by the spin period P_s and the Bragg grating period Λ , and superimposed in an

FBG. Based on this mechanism and the proposed CMEs [11], the FBG spectra of reflection and transmission are then simulated and plotted in Fig. 9(b) for a nonpolarized input light (an integral of all linear SOP), where we take $P_s = 1.78$ mm, $\Lambda = 532.41$ μm , $\Delta n_L = 0.378 \times 10^{-4}$, an FBG length of 15 mm, AC and DC grating index changes of 0.3×10^{-4} and 2.8×10^{-4} , and a sinusoidal modulation with an amplitude of 0.27×10^{-4} caused by the spiral stress. We can see that five peaks, P_B , $P_{\pm 1}$, and $P_{\pm 2}$, are dominant, and the amplitudes of $P_{\pm 3}$ are weaker than those of $P_{\pm 4}$. The simulation result is qualitatively consistent with the measured one, and their deviations are attributed to the assumption of the grating index distribution that cannot be precisely measured under our current experimental conditions. When linearly polarized inputs with different SOP were calculated in the simulation, it was found that the FBG reflectivity varied by ~ 0.1 dB for P_B , ~ 2.0 dB for $P_{\pm 1}$, and ~ 5.0 dB for $P_{\pm 2}$. Such polarization dependences were also observed for circularly and elliptically polarized waves. In addition, the measured results show that in the grating transmission bands, these spun FBGs with a typical grating length of 15 mm have very low PMD (~ 0.01 ps) and polarization-dependent losses (PDL, < 0.03 dB) including 350-mm lead fibers, which makes these spun FBGs also suitable for many high-speed communication systems.

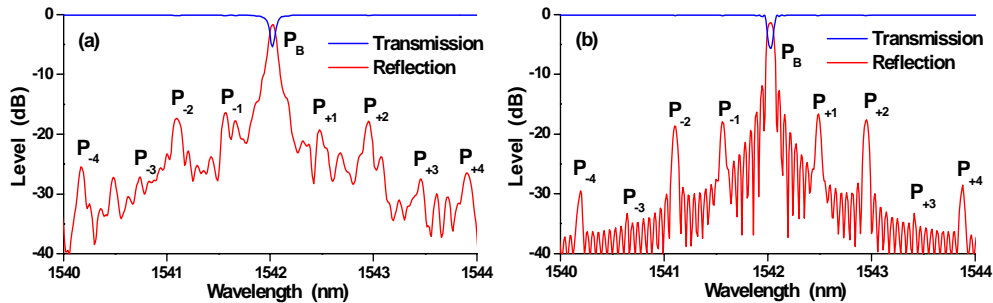


Fig. 9. (a) Measured and (b) simulated FBG spectra for Fiber #2

Such strong polarization dependences of the side peaks and low dependence of the Bragg peak in the reflection spectrum offer an outstanding property for potential applications in novel fiber sensing. For example in some fiber temperature, strain and pressure sensing systems, temperature or strain information can be read out from λ_B [12]; while the changes of SOP can be examined with respect to reflectivity variations of the side peaks, which may be used to monitor pressure or other parameters.

In consideration of these applications, there are some basic requirements for parameter selection of spun fibers. The major two parameters are the spin period P_s and intrinsic birefringence Δn_L , which can affect the amplitudes and intervals of side peaks. Based on the sampled FBG theory [12], the wavelength interval $\Delta\lambda$ of side peaks is equal to $\lambda_B \cdot \Lambda / P_s$, which in turn provides a novel method for precise measurement of short spin period. With a 0.01 nm resolution in the spectrum measurement, the spatial resolution of spin period is correspondingly ~ 0.1 mm, which can be further improved by using a high-resolution tunable laser source. For a typical 1550-nm FBG, the wavelength interval varying with spin period is shown in Fig. 10(a). Particularly for $0.1 < \Delta\lambda < 1.0$ nm, the spin period should range in 0.8 ~ 8.0 mm. A too large or a too small $\Delta\lambda$ is usually inappropriate for the sensing applications. This is because the former will reduce the capability of wavelength-division multiplexing within a certain bandwidth; while the latter may cause difficulty in distinguishing neighboring two side peaks. Hence, a value of $\Delta\lambda$ in the range 0.1-1.0 nm is preferred, corresponding to a spin period at a millimeter level. It is found that the amplitudes of side peaks depend strongly on intrinsic birefringence Δn_L as well as grating length and AC index change, and weakly on spin period. For typical 1550-nm FBGs with a length of 15 mm and an AC index change of

0.5×10^{-4} in spun fiber #2, the amplitudes of the major four side peaks in the reflection spectrum are shown in Fig. 10(b) as functions of Δn_L , where a nonpolarized input is adopted to avoid the polarization dependence of spectrum on input SOP described previously. We can see that with a decrease of Δn_L , the amplitudes of the side peaks drop significantly. As usual, allowable minimum amplitudes of the side peaks rely on the intensity of light source and sensitivity of detection system; the stronger the side peaks, the higher the signal-to-noise ratio. Typically in Fig. 10(b), Δn_L should be greater than 0.36×10^{-4} for $P_{\pm 1} > -15$ dB, and 0.25×10^{-4} for $P_{\pm 2} > -20$ dB. It is hence concluded that a spun fiber with 0.3×10^{-4} birefringence and a millimetre spin period is preferable for these sensing applications.

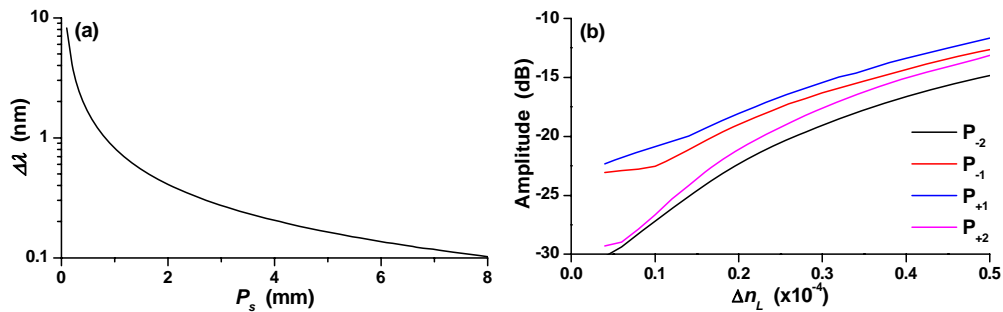


Fig. 10. (a) Wavelength interval of FBG side peaks versus spin period. (b) Amplitudes of side peaks versus fiber birefringence for spun fiber #2.

5. Conclusion

The spun fibers with intrinsic asymmetric stress and millimeter spin periods have been characterized in terms of experiment and theory. The longitudinal spiral distributions of stress were confirmed under direct observation and with the aid of imprinted fiber Bragg gratings. In determination of spun fiber parameters, by measuring reflection spectra of imprinted fiber Bragg gratings, we precisely acquired spin periods with a 0.1-mm spatial resolution; meanwhile, by comparing the measured and simulated fiber PMD, we obtained accurate intrinsic birefringence of spun fibers, which is lower than that of the unspun fiber by a factor of 3. Both the experimental and simulation results show that the spinning process of fiber with millimeter spin periods can significantly reduce fiber PMD by a factor of over 10, and the fiber PMD exhibits a linear relation with fiber length. To effectively reduce fiber PMD for long-haul and high-speed applications in telecommunications, spun fibers with low intrinsic birefringence and short spin period are usually required. Due to the mode conversion and averaging effect in spun fibers, the introduced linear birefringence can enable these spun fibers to have a good resistance to external perturbations, and render polarization-insensitive transmissions possible. Due to the presence of the superstructure in a spun fiber grating, the multiple peaks appear near the Bragg wavelength in the reflection spectrum. Strong polarization dependences of the side peaks and weak dependence of the Bragg peak on input SOP render the spun fiber gratings attractive in novel fiber sensing.

Acknowledgments

This work is supported by the Ontario Photonics Consortium (OPC), the Photonics Research Ontario (PRO), the Natural Sciences and Engineering Research Council of Canada (NSERC) and the Canada Foundation for Innovation (CFI) under New Opportunities program. The authors would like to thank their colleagues Dr. C. Yang and X.-P. Dong, and Dr X. Chen of Corning Inc. for helpful discussions, Dr. X.-J. Gu of Ryerson University for help in hydrogen loading of fibers, and Dr. X.-Z. Chen and Dr. X. Li of McMaster University for lending the measurement instruments.